

Filling Box Flows in an Axisymmetric Porous Medium

Chunendra K. Sahu · M. R. Flynn

Received: date / Accepted: date

Abstract We present an analytical solution for buoyancy-driven “filling box” flows in axisymmetric porous media having closed bottom and side boundaries. The flow consists first and foremost of a descending, point source plume. When plume fluid reaches the (horizontal) bottom boundary, it begins to flow radially outward in the form of an axisymmetric gravity current. The leading edge of the gravity current advances with time as $t^{1/2}$ until it reaches the vertical sidewalls. At this point, the flow is characterized by a vertically-ascending “first front” that steadily advects towards the plume source. We assume the plume to be in a Darcy regime, i.e. $Re \lesssim \mathcal{O}(10)$, with $Pe > \mathcal{O}(1)$, where Re and Pe are respectively the Reynolds and Péclet numbers, and derive a similarity solution for the plume by applying a boundary layer approximation. Formulas are thereby obtained for the vertical variation of the plume volume flux and area-averaged concentration. The former result shows important qualitative differences with the analogue equation derived in the limit $Pe < \mathcal{O}(1)$. In particular, the plume volume flux is now predicted to explicitly depend on the reservoir permeability, plume buoyancy flux and fluid viscosity. The gravity current problem is likewise solved using a self-similar solution, this time adapted from the work of Lyle et al. (*J. Fluid Mech.* vol. 543, 293–302, 2005) but connected to the outflow conditions of the plume. Finally, in solving for the motion of the first front, we apply a volume flux balance equation and thereby estimate the time scale required for the first front to advect from the bottom of the control volume to the source elevation. By synthesizing the above results,

C. K. Sahu
E-mail: chunendra@ualberta.ca
Dept. of Mechanical Engineering and Inst. for Geophysical Research, University of Alberta,
T6G 1H9, Canada

M. R. Flynn
E-mail: mrflynn@ualberta.ca
Dept. of Mechanical Engineering and Inst. for Geophysical Research, University of Alberta,
T6G 1H9, Canada

we can estimate the total volume of source fluid and mass of solute that can be injected into an axisymmetric reservoir without overflow. Predictions can also be made for the time-variable mean concentration of this contaminated fluid layer, which must obviously be less than the source concentration.

Keywords Porous media · Filling box flows · Buoyant convection · Plumes/thermals · Gravity currents · Dispersion/diffusion

1 Introduction

The term “filling box flows” was first coined by Baines & Turner in 1969 [2] in their study of buoyant convection from an isolated source in a closed cylindrical control volume devoid of porous media. Since then filling box flows have been studied extensively because of their applicability to numerous environmental and industrial scenarios, e.g. in volcanic and submarine pumice eruptions [23], hydrothermal plumes [20] and building ventilation [9]. A recent theoretical and similitude laboratory experimental extension of the filling box methodology has been to the case of porous media plumes that rise or fall within “leaky” [16] or closed [17] aquifers. The latter case is of particular interest because of its applicability to numerous geophysical and industrial scenarios, for instance, (i) injection of hot water underground for the purpose of thermal storage in a confined reservoir [5], (ii) injection, and subsequent dissolution, of supercritical CO₂ into deep saline aquifers for purposes of sequestering the CO₂ that is produced as a result of localized industrial activities, e.g. coal combustion for power generation [3], (iii) dense plumes generated as a result of leakages from landfills, waste piles or composting facilities that subsequently contaminate potable groundwater [7, 12, 13], (iv) disposal by re-injection of the produced water associated with either shale gas or heavy oil activities [1, 19]. In each case, a comprehensive analytical description of the flow requires combination of vertical convection and the primarily horizontal flow that follows when plume fluid reaches an impermeable horizontal boundary.

In this spirit, a central objective of the present contribution is to expand upon existing descriptions of porous media filling box flows by extending the Cartesian analysis employed in Sahu & Flynn [17] to an axisymmetric geometry. Such an extension is not at all trivial; for instance, it provides an opportunity to supplement a well-established, but physically counter-intuitive, expression for the plume volume flux – see (1) and the corresponding discussion below. A further objective of our research is to clarify the mathematical treatment of the different components of the dispersion tensor under the boundary layer approximation and thereby justify, more carefully than before, why some of these terms can be safely ignored.

As suggested by the schematics of figure 1, we divide our problem into three constituent parts comprising the plume, gravity current and the first front. Although the plume shown in figure 1 is negatively-buoyant, it should be understood that dynamically equivalent results are expected if the plume rises rather than falls, provided, of course, that the flow is Boussinesq, i.e. density

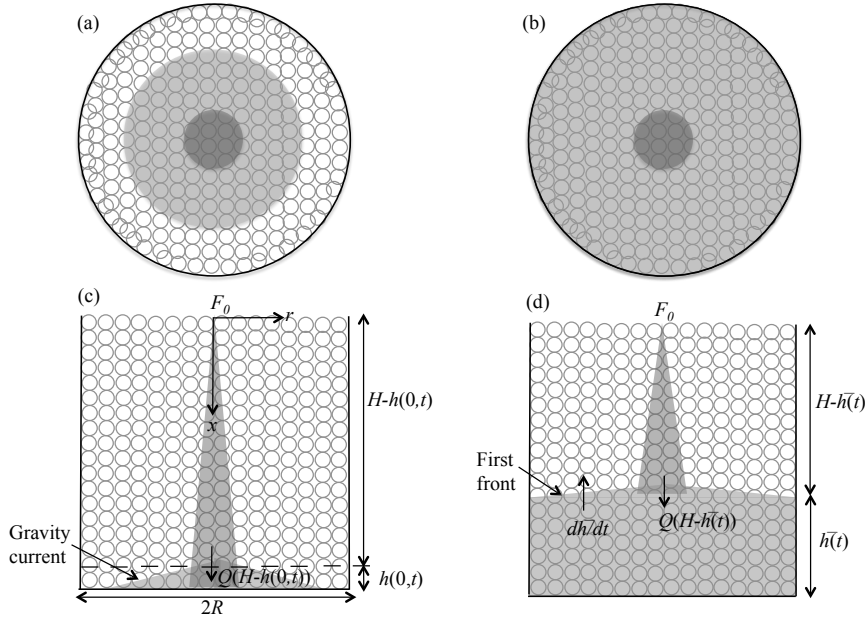


Fig. 1: Schematic of a filling box flow in an axisymmetric geometry. (a) and (c) represent, respectively, the top view and front view of the plume and gravity current. (b) and (d) represent, respectively, the top and front view of the plume and the first front.

differences are less than about 10%. Note that in either orientation, we assume that the plume originates from a compact source and thereafter propagates through a uniform porous medium. The gravity current describes the radially outward motion of the discharged plume fluid over an impermeable horizontal boundary. Unlike the studies of Neufeld et al. [10] and Roes et al. [16], we do not include any localized sinks in this bottom boundary and so the gravity current outflow is uniform in all directions. Finally the first front describes the primarily vertical motion of this discharged plume fluid after the leading edge of the gravity current has reached the impermeable vertical walls that define the sidewalls of the control volume.

A solution for axisymmetric plumes falling through an unbounded porous medium can be derived from a Wooding (1963)-type [22] boundary layer approximation using a constant value for the dispersion coefficient. On this basis, and supposing that dispersion is, in fact, dominated by molecular diffusion effects, the plume volume flux, Q , can be shown to vary with the vertical distance, x , from the source as

$$Q = 8\pi D_d \phi x. \quad (1)$$

(see equation 7.5.34 of Phillips [15], section 9.10 of Turcotte & Schubert [21] and equation 3.1 of Roes et al. [16]). Here D_d is the solute molecular diffusion

coefficient and ϕ is the porosity. This equation is notable for several reasons. Firstly, and as suggested above, it assumes that mechanical dispersion is subordinate to molecular diffusion. Thus the Péclet number, which is defined as the ratio of mass transfer by mechanical dispersion to mass transfer by diffusion, is $Pe = \frac{dU\tau}{D_d} < \mathcal{O}(1)$, where d is the mean grain size, U is the transport velocity and $\tau (> 1)$ is the tortuosity constant, which is defined as the ratio of the actual path length traveled by a solute molecule to the distance it would travel in a free medium. Conversely when $Pe > \mathcal{O}(1)$, a situation not at all uncommon in practice, mechanical dispersion effects dominate over molecular diffusion and must therefore be taken into account when evaluating the mass transfer. In this case, the diffusion coefficient must be replaced by a dispersion tensor whose components depend on the flow velocity. More specifically, the components of the dispersion tensor are associated with the normal and tangential directions of the longitudinal and radial components of the velocity field as explained by Ogata [11] and reviewed in greater detail below.

Equation (1) is also notable for the fact that Q is independent of the plume buoyancy flux, F . This prediction, though mathematically consistent, is quite different from the corresponding result for a line source plume for which

$$Q = \left(\frac{36D_d\phi Fk\Lambda^2 x}{\nu} \right)^{1/3} \quad (2)$$

where Λ is the width of the line source, k is the permeability and ν is the kinematic viscosity [15]. Note, moreover, that free plumes, whether axisymmetric or 2D planar both predict Q to vary with F – see e.g. (5) and (16) of Baines & Turner [2]. Equations (1) and (2) also differ in that the plume volume flux depends on k and ν only in the latter instance. Thus one of the strong motivations for extending the analysis of Sahu & Flynn [17] to the case of an axisymmetric plume issuing from a point source is to determine whether the unusual functional form of (1) is somehow preserved. Indeed, as we illustrate below, by specifically considering $Pe > \mathcal{O}(1)$, it is possible to derive a self-similar solution for Q that more closely conforms to (2) and the related expressions from free plume theory.

The second part of the filling box flow consists of a gravity current, which is formed when dense plume fluid reaches the bottom impermeable boundary. In this case, the plume acts as a distributed source of dense fluid for the axisymmetric gravity current; the plume volume flux and mean reduced gravity at the bottom of the control volume are therefore needed in order to correctly specify the gravity current inflow conditions. Lyle et al. (2005) studied the axisymmetric gravity current problem both theoretically and experimentally, but in a radially infinite ambient. We adopt their theoretical solution, couple it with the equations describing the descending plume and finally present a solution for the horizontal motion of the discharged plume fluid in a finite ambient.

Note finally that as the gravity current propagates radially outward, it gets progressively thinner. At a particular point in time, t_R , the (well-defined)

leading edge of the gravity current reaches the cylindrical sidewall. We develop estimates for t_R and also the height profile of the gravity current at this instant in time. The latter piece of information is needed when modelling the subsequent motion of the discharged plume fluid back towards the plume source. This primarily vertical motion is characterized by a so-called first front, which separates dense fluid below from fresh ambient fluid above. The shape of this first front obviously matches that of the gravity current when $t = t_R$ but its slope subsequently decreases as the first front advects upwards. We follow the approach of volume flux balance, presented by Sahu & Flynn [17] for the recilinear case, and derive an equation that describes the temporal evolution of the first front. Thus the motion of the first front will be shown to depend on both the solution of the plume and the gravity current problems.

The rest of the manuscript is organized as follows: we present a theoretical solution for the plume, gravity current and first front in sections 2, 3 and 4, respectively. Thereafter section 5 shows the output of our composite analytical model, discusses the key time scales associated with a filling box flow and identifies conditions associated with a maximal filling of the control volume. Finally, section 6 summarizes the work as a whole and briefly identifies topics for further study.

2 Plume

The flows exhibited schematically in figure 1 are assumed to be both Boussinesq and miscible. Flow speeds are small enough that the flow remains laminar but large enough so that $Pe > \mathcal{O}(1)$. We further assume that the porous medium is uniform and saturated. Therefore the governing equations, i.e. mass continuity, momentum conservation in x and r , solute transport by advection-dispersion and a (linear) equation of state, are respectively given by

$$\frac{\partial u}{\partial x} + \frac{\partial v}{\partial r} = 0, \quad (3)$$

$$\frac{1}{\rho_0} \frac{\partial P}{\partial x} + \frac{\nu}{k} u = \frac{g\rho}{\rho_0}, \quad (4)$$

$$\frac{1}{\rho_0} \frac{\partial P}{\partial r} + \frac{\nu}{k} v = 0, \quad (5)$$

$$\frac{1}{\phi} \left[u \frac{\partial C}{\partial x} + v \frac{\partial C}{\partial r} \right] = \frac{\partial}{\partial x} \left(D_{xx} \frac{\partial C}{\partial x} + D_{xr} \frac{\partial C}{\partial r} \right) + \frac{1}{r} \frac{\partial}{\partial r} \left(D_{rx} r \frac{\partial C}{\partial x} + D_{rr} r \frac{\partial C}{\partial r} \right) \quad (6)$$

$$\rho = \rho_\infty (1 + \beta C). \quad (7)$$

Here u and v are the transport velocities in the axial and radial directions, respectively. Meanwhile, P is the fluid pressure, C is the solute concentration, β is the solute contraction coefficient and ρ is the fluid density, which approaches a constant value of ρ_∞ in the far-field limit, $r \rightarrow \infty$. Furthermore, D_{xx} , D_{xr} , D_{rx} and D_{rr} are respectively the components of the axial and radial dispersion coefficients in the tangential and normal directions.

By combining (4) and (5), it can be shown that

$$\frac{\nu}{k} \left(\frac{\partial u}{\partial r} - \frac{\partial v}{\partial x} \right) = \frac{g}{\rho_0} \frac{\partial \rho}{\partial r}. \quad (8)$$

Next, by applying the former of Wooding's two boundary layer conditions [22], we conclude

$$\left| \frac{\partial v}{\partial x} \right| \ll \left| \frac{\partial u}{\partial r} \right|. \quad (9)$$

Incorporating (7) and (9) into (8) gives

$$\frac{\partial u}{\partial r} = \frac{g\beta k}{\nu} \frac{\partial C}{\partial r}. \quad (10)$$

Regarding the right-hand side of (6) and following Scheidegger [18], the dispersion coefficients can be defined in terms of the axial velocity as follows: $D_{xx} = \alpha_{xx}u$, $D_{xr} = \alpha_{xr}u$, $D_{rx} = \alpha_{rx}u$ and $D_{rr} = \alpha_{rr}u$, where α_{xx} , α_{xr} , α_{rx} and α_{rr} are the corresponding dispersivity constants whose values vary between 0.01 to 1 cm [4]. Therefore (6) can be written as

$$\frac{1}{\phi} \left[u \frac{\partial C}{\partial x} + v \frac{\partial C}{\partial r} \right] = \frac{\partial}{\partial x} \left[u \left(\alpha_{xx} \frac{\partial C}{\partial x} + \alpha_{xr} \frac{\partial C}{\partial r} \right) \right] + \frac{1}{r} \frac{\partial}{\partial r} \left[ur \left(\alpha_{rx} \frac{\partial C}{\partial x} + \alpha_{rr} \frac{\partial C}{\partial r} \right) \right]. \quad (11)$$

Scheidegger [18] further suggests that the tangential components of the dispersivity are larger than the normal components, and therefore $\alpha_{xx} \gg \alpha_{xr}$ and $\alpha_{rr} \gg \alpha_{rx}$. Also, from Wooding's latter boundary layer condition [22], we have

$$\left| \frac{\partial C}{\partial x} \right| \ll \left| \frac{\partial C}{\partial r} \right|. \quad (12)$$

Thus, it can be shown that

$$\left| \alpha_{xx} \frac{\partial C}{\partial x} \right| \sim \left| \alpha_{xr} \frac{\partial C}{\partial r} \right| \quad \text{and} \quad \left| \alpha_{rx} \frac{\partial C}{\partial x} \right| \ll \left| \alpha_{rr} \frac{\partial C}{\partial r} \right|. \quad (13)$$

However, on performing a scaling analysis and remembering that axial length scales are much larger than their radial counterparts, we find

$$\left| \frac{\partial}{\partial x} \left(u \alpha_{xr} \frac{\partial C}{\partial r} \right) \right| \sim \left| \frac{1}{r} \frac{\partial}{\partial r} \left(ur \alpha_{rx} \frac{\partial C}{\partial x} \right) \right|, \quad (14)$$

which suggests that only the final term on the right hand side of (11) is dynamically significant. In other words, (11) can be rewritten in the following approximate form:

$$u \frac{\partial C}{\partial x} + v \frac{\partial C}{\partial r} = \frac{\phi}{r} \frac{\partial}{\partial r} \left(ur \alpha_{rr} \frac{\partial C}{\partial r} \right). \quad (15)$$

Hereafter we refer α_{rr} to simply as α .

We now introduce a streamfunction, ψ , such that $u = \frac{1}{r} \frac{\partial \psi}{\partial r}$ and $v = -\frac{1}{r} \frac{\partial \psi}{\partial x}$. Therefore on further substitution, (10) and (15) respectively become

$$\frac{1}{r} \frac{\partial^2 \psi}{\partial r^2} - \frac{1}{r^2} \frac{\partial \psi}{\partial r} = \frac{g\beta k}{\nu} \frac{\partial C}{\partial r}, \quad (16)$$

$$\frac{\partial \psi}{\partial r} \frac{\partial C}{\partial x} - \frac{\partial \psi}{\partial x} \frac{\partial C}{\partial r} = \alpha \phi \left(\frac{\partial^2 \psi}{\partial r^2} \frac{\partial C}{\partial r} + \frac{\partial \psi}{\partial r} \frac{\partial^2 C}{\partial r^2} \right). \quad (17)$$

We seek a self-similar solution to (16) and (17) of the form

$$\psi = A_1 x^p \mathcal{F}(\eta), \quad C = A_2 x^q \mathcal{G}(\eta) \quad (18)$$

where $\eta = A_3 \frac{r}{x^m}$ is the self-similar variable and A_1 , A_2 and A_3 are constants to be determined shortly. Substituting (18) into (16) and further simplifying gives

$$\eta \mathcal{F}'' - \mathcal{F}' = \frac{g\beta k}{\nu} \frac{A_2}{A_1} \frac{r^2 x^q}{x^p} \mathcal{G}' = \frac{g\beta k}{\nu} \frac{A_2}{A_1 A_3^2} \left[\frac{A_3 r}{x^{(p-q)/2}} \right]^2 \mathcal{G}' \quad (19)$$

Self-similarity requires that $p-q = 2m$ so that $\eta = A_3 \frac{r}{x^{(p-q)/2}}$ and $A_2 = \frac{\nu}{g\beta k} A_1 A_3^2$.

Upon making these substitutions, (19) simplifies dramatically, i.e.

$$\eta \mathcal{F}'' - \mathcal{F}' = \eta^2 \mathcal{G}'. \quad (20)$$

From (18), and remembering that the solute concentration is maximal at $r = 0$ and vanishingly small when $r \rightarrow \infty$, we have the following boundary conditions to be applied in conjunction with (20): $\mathcal{G}' = 0$ at $\eta = 0$ and $\mathcal{G} = 0$ when $r \rightarrow \infty$. We shall apply the former boundary condition later; employing the latter boundary condition now, it can be shown that (20) has a general solution of the form

$$\mathcal{G} = \frac{\mathcal{F}'}{\eta}. \quad (21)$$

We now repeat the above process but focus attention on (17) rather than (16). Substituting (18) into (17), it can be shown that

$$\mathcal{F}'(q\mathcal{G} - m\mathcal{G}'\eta) - (p\mathcal{F} - m\mathcal{F}'\eta)\mathcal{G}' = \alpha \phi x^{(1-2m)} A_3^2 (\mathcal{F}''\mathcal{G}' + \mathcal{F}'\mathcal{G}''). \quad (22)$$

By selecting $m = 1/2$ and $A_3 = 1/\sqrt{\alpha\phi}$, (22) reduces to the following simpler form:

$$\mathcal{F}''\mathcal{G}' + \mathcal{F}'\mathcal{G}'' - q\mathcal{F}'\mathcal{G} + p\mathcal{F}\mathcal{G}' = 0. \quad (23)$$

To determine p and q , we recall that the buoyancy flux, F , is constant and equal to its source value, F_0 . Thus

$$2\pi \int_0^\infty u g' r \, dr = F_0. \quad (24)$$

Here $g' = g \frac{\rho - \rho_\infty}{\rho_\infty} = g\beta C$ is the reduced gravity of the plume. Substituting (18) into (24), shows that

$$2\pi x^{p+q} A_1 A_2 g \beta \int_0^\infty \mathcal{F}' \mathcal{G} dr = F_0, \quad (25)$$

and this in turn implies $p + q = 0$. Recalling $p - q = 2m = 1$, we conclude that $p = 1/2$ and $q = -1/2$. Also, with reference to (25), and remembering that $A_2 = \frac{\nu}{g\beta k} A_1 A_3^2$ and $A_3 = 1/\sqrt{\alpha\phi}$, it is easy to verify that

$$A_1 = \left(\frac{F_0 k \alpha \phi}{2\pi \nu} \frac{1}{\int_0^\infty \mathcal{F}' \mathcal{G} d\eta} \right)^{1/2}.$$

Using the above results, (23) takes the form

$$\mathcal{F}'' \mathcal{G}' + \mathcal{F}' \mathcal{G}'' + \frac{1}{2} \mathcal{F}' \mathcal{G} + \frac{1}{2} \mathcal{F} \mathcal{G}' = 0. \quad (26)$$

After combining (21) and (26), and with some algebra, we get

$$\mathcal{G}'' + \frac{\mathcal{G}'}{\eta} + \mathcal{G} = 0. \quad (27)$$

\mathcal{G} therefore represents a Bessel function of first kind, $J_0(\eta)$, and can be expressed in integral form as

$$\mathcal{G} = J_0(\eta) = \frac{2}{\pi} \int_0^{\pi/2} \cos(\eta \sin \theta) d\theta. \quad (28)$$

Before applying this solution to the problem at hand, we recall the assumption that $\text{Pe} > \mathcal{O}(1)$, or $D_{rr} = \alpha u$. In the region close to the plume centerline where flow velocities are comparatively large, this approximation is certainly appropriate, however, the above assumption breaks down as we move to the far-field, which is characterized by much smaller vertical (and radial) velocities. We therefore divide our solution into an inner region where $\text{Pe} > \mathcal{O}(1)$ and an outer region where $\text{Pe} \leq \mathcal{O}(1)$. In determining the appropriate boundary between the inner and outer region, recall that \mathcal{G} represents the solute concentration (see equation 18), whose value cannot become negative. Therefore the inner region is formally defined by $\eta \leq \eta_{\max} = 2.4048$ for which $\mathcal{G} \geq 0$ [24]. In the outer region, we assume, consistent with the analysis of Sahu & Flynn [17], that the fluid velocity and solute concentration are identically zero. Thus, in place of (27), it is more appropriate to write

$$\mathcal{G} = \begin{cases} \frac{2}{\pi} \int_0^{\pi/2} \cos(\eta \sin \theta) d\theta, & \eta \leq \eta_{\max} \\ 0, & \eta > \eta_{\max}. \end{cases} \quad (29)$$

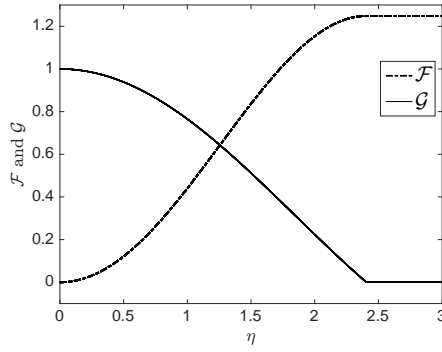


Fig. 2: Analytical solution obtained for the self-similar functions \mathcal{G} and \mathcal{F} of (18) vs. the self-similar variable, η .

Furthermore, by considering the relationship between \mathcal{G} and \mathcal{F}' from (21), the solution for \mathcal{G} can be extended to find \mathcal{F} such that

$$\mathcal{F} = \begin{cases} \frac{2}{\pi} \int_0^\eta \int_0^{\pi/2} \cos(\eta \sin \theta) d\theta d\eta, & \eta \leq \eta_{\max} \\ 1.2485, & \eta > \eta_{\max}. \end{cases} \quad (30)$$

The variation of \mathcal{F} and \mathcal{G} with η are presented in figure 2. By combining (29) and (30) with (18), a contour plot may be drawn that shows the variation of u/u_0 or, equivalently, C/C_0 with x/H and r/H where u_0 and C_0 are the plume vertical velocity and solute concentration at the source and H is the control volume height – see figure 3. Note that u and C therefore vary in proportion to one another.

With a formula for ψ to hand, it is straightforward to evaluate the plume volume flux, Q , i.e.

$$Q = 2\pi \int_0^\infty u dr = \left[2\pi \frac{F_0 k \alpha \phi}{\nu} \frac{(\int_0^\infty \mathcal{F}' d\eta)^2}{\int_0^\infty \frac{\mathcal{F}'^2}{\eta} d\eta} x \right]^{1/2}. \quad (31)$$

From the solution presented in figure 2, we have $\frac{(\int_0^\infty \mathcal{F}' d\eta)^2}{\int_0^\infty \frac{\mathcal{F}'^2}{\eta} d\eta} = 2$. Thus the volume flux for an ideal plume with $\text{Pe} > \mathcal{O}(1)$ and $D_{rr} = \alpha u$ is given simply by

$$Q = \left(\frac{4\pi F_0 k \alpha \phi}{\nu} x \right)^{1/2}. \quad (32)$$

On comparing this result with (1), our result shows that the plume volume flux depends not only on the porosity, but also on the plume buoyancy flux, the reservoir permeability and the fluid kinematic viscosity, all of which seems very reasonable on physical grounds. Another potentially significant difference

with (1) is that this previous equation predicts $Q \propto x$, whereas our solution predicts a more conservative result, namely $Q \propto x^{1/2}$.

Because the plume buoyancy flux is constant, it is straightforward to obtain an expression for the plume mean reduced gravity, averaged over the cross section. The corresponding formula,

$$\bar{g}' = g\beta\bar{C} = \left(\frac{F_0\nu}{4\pi k\alpha\phi} \frac{1}{x} \right)^{1/2}, \quad (33)$$

unambiguously specifies the connection between \bar{g}' , \bar{C} , F_0 and x . For (32) and (33) to be applicable to a nonideal plume, for which the source volume flux is not vanishingly small, we back-extrapolate our result so that $Q = 0$ at a virtual source defined by $x = -x_0$ [6], [22]. Thus

$$x_0 = \frac{\nu Q_0^2}{4\pi F_0 k\alpha\phi} = \frac{\nu Q_0}{4\pi g'_0 k\alpha\phi}, \quad (34)$$

where g'_0 is the reduced gravity of the source fluid. Therefore for a nonideal plume, the volume flux and mean reduced gravity are given, respectively, by

$$Q = \left[\frac{4\pi F_0 k\alpha\phi}{\nu} (x + x_0) \right]^{1/2}. \quad (35)$$

and

$$\bar{g}' = g\beta\bar{C} = \left[\frac{F_0\nu}{4\pi k\alpha\phi} \frac{1}{(x + x_0)} \right]^{1/2}. \quad (36)$$

Substituting x_0 using (34) and expressing (35) and (36) in non-dimensional form yields

$$\frac{Q}{Q_0} = \left[1 + \frac{4\pi g'_0 k\alpha\phi H}{Q_0\nu} \left(\frac{x}{H} \right) \right]^{1/2} \quad \text{and} \quad \frac{\bar{g}'}{g'_0} = \left[1 + \frac{4\pi g'_0 k\alpha\phi H}{Q_0\nu} \left(\frac{x}{H} \right) \right]^{-1/2}, \quad (37)$$

The functional variation of Q/Q_0 and \bar{g}'/g'_0 is depicted in the left- and right-hand side panels of figure 4, respectively.

The above results apply to a time-independent flow and so do not fully capture the dynamics associated with the initiation of dense source fluid and the thermal that results therefrom. Plumes and thermals share some similarities, of course, but also some important differences. In the former case, for instance, entrainment occurs only laterally whereas in the latter case, ambient fluid may also be entrained along the descending underside of the thermal. With this caveat in mind, we nonetheless proceed to estimate, on the basis of the previous formulas, the time interval, t_P , between activating the source and observing plume fluid along the lower impermeable boundary of the control volume. The average axial plume velocity at any arbitrary elevation is given by

$$U(x) \equiv \frac{Q(x)}{A_p} = \left[\frac{4F_0 k}{\eta_{\max}^4 \pi \nu \alpha \phi} \frac{1}{(x + x_0)} \right]^{1/2} \quad (38)$$

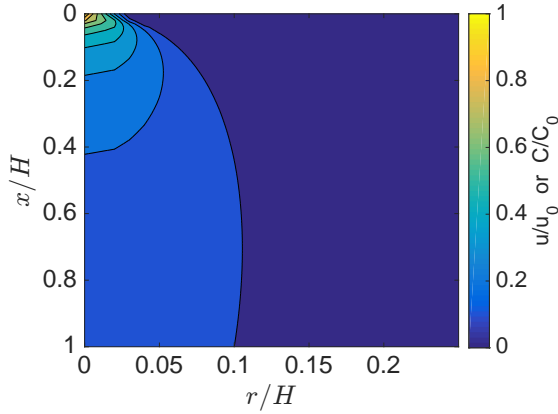


Fig. 3: [Colour online] Contours showing the variation of u/u_0 or C/C_0 with x/H and r/H where u_0 and C_0 are respectively the plume vertical velocity and solute concentration at the source.

where the plume cross-sectional area is given by $A_p = \pi b^2 = \pi \alpha \phi \eta_{\max}^2 x$. By extension, the mean value of $U(x)$ in a control volume having height H is given by

$$\bar{U} = \frac{1}{H} \int_0^H U(x) dx = \left(\frac{16F_0 k}{\pi \eta_{\max}^4 \nu \alpha \phi} \right)^{1/2} \left[(H + x_0)^{1/2} - x_0^{1/2} \right]. \quad (39)$$

Employing this result, the time required for the plume to traverse a vertical distance H is estimated as

$$t_P = \left(\frac{\pi \eta_{\max}^4 \nu \alpha \phi}{16F_0 k} \right)^{1/2} \frac{H}{\left[(H + x_0)^{1/2} - x_0^{1/2} \right]}. \quad (40)$$

Below, we shall compare t_P against other relevant time-scales of the flow e.g. those due to the gravity current and ascending first front.

3 Gravity current

As the dense plume reaches the impermeable bottom of the cylindrical control volume, it transitions to a gravity current and propagates radially outward. Assuming a hydrostatic pressure condition, and adapting the self-similar solution presented by Lyle et al. [8], we may describe the motion of the gravity current as outlined below.

According to Darcy's law, the outward radial velocity of the discharged dense fluid can be expressed as a function of the slope of the interface that

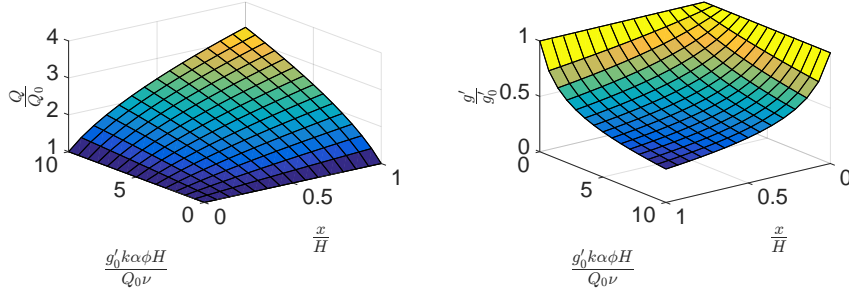


Fig. 4: [Colour online] Variation of Q/Q_0 (left-hand side panel) and \bar{g}/g'_0 (right-hand side panel) with x/H and $g'_0 k \alpha \phi H / (Q_0 \nu)$ – see (37).

separates this fluid from the overlying ambient, i.e.

$$v_g = -\frac{k g'_g}{\nu} \frac{\partial h}{\partial r}. \quad (41)$$

Here h is the interface height as depicted in figure 1 and g'_g is the mean reduced gravity calculated at $x = H$ using (36).

Local volume flux balance states that the difference of the volumetric inflow and outflow at any radial location r must be balanced by the time rate of change of the interface height at the same location. Expressing this balance mathematically yields

$$\phi \frac{\partial h}{\partial t} + \frac{1}{r} \frac{\partial}{\partial r} (r v_g h) = 0. \quad (42)$$

On combining (41) and (42), we find that

$$\frac{\partial h}{\partial t} - \frac{S}{r} \frac{\partial}{\partial r} \left(r h \frac{\partial h}{\partial r} \right) = 0, \quad (43)$$

where $S = \frac{k g'_g}{\nu \phi}$. The above equation is a nonlinear heat equation and is subject to the following boundary conditions:

$$h(r_N, t - t_P) = 0 \quad \text{and} \quad 2\pi\phi \int_0^{r_N(t-t_P)} r h(r, t - t_P) dr = V_g(t - t_P). \quad (44)$$

Here r_N is the radial distance measured from the origin to the gravity current leading edge (or nose) and V_g is the total volume of fluid discharged by the plume up till time $t - t_P > 0$. The former boundary condition states that the height of the gravity current at its leading edge is always zero. By contrast, the latter boundary condition states that the amount of the dense fluid contained

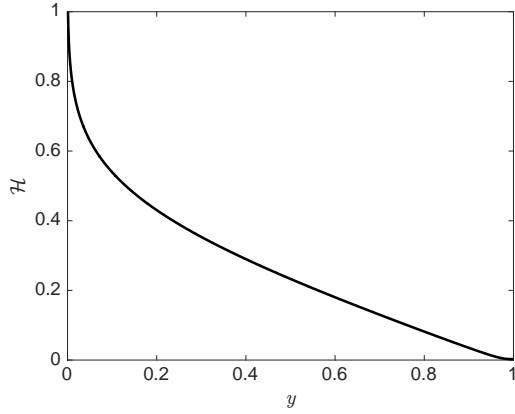


Fig. 5: Dimensionless gravity current height \mathcal{H} vs dimensionless radius y .

within the gravity current must equal V_g . Following Lyle et al.'s approach, we define a self-similar solution of the form

$$h(r, t - t_P) = \xi_N^2 \left(\frac{Q_g}{S} \right)^{1/2} \mathcal{H}(y) \quad \text{where} \quad \xi(r, t - t_P) = \frac{r}{(SQ_g)^{1/4} (t - t_P)^{1/2}}. \quad (45)$$

Here $0 \leq y = \xi/\xi_N \leq 1$ and $\xi_N = \xi(r_N, t - t_P)$ is the dimensionless radius of the leading edge. On substituting (45) into (43), we obtain

$$y\mathcal{H}''\mathcal{H} + y\mathcal{H}'\mathcal{H}' + \mathcal{H}'\mathcal{H} + \frac{y^2}{2}\mathcal{H}' = 0, \quad (46)$$

subject to the boundary conditions

$$\mathcal{H}(1) = 0 \quad \text{and} \quad \left[2\pi \int_0^1 y\mathcal{H} dy \right]^{-1/4} = \xi_N. \quad (47)$$

To find a solution to the above ODE, a shooting method is employed. Graphical results are presented in figure 5 and the value of ξ_N is found to equal 1.19. These results match very well with figures 2 and 3 of Lyle et al. [8].

Using the above equations, the radius of the gravity current as a function of time $t > t_P$ can be given as

$$r_N = \xi_N (SQ_g)^{1/4} (t - t_P)^{1/2}. \quad (48)$$

On the other hand, the time required for the gravity current to reach the sidewalls of the cylindrical control volume, located at $r = R$, can be found from

$$t_R = \frac{R}{\xi_N (SQ_g)^{1/4}}, \quad (49)$$

where we assume that the plume radius at $x = H$ is negligible compared to R . In light of this definition, (48) can be simplified to read

$$\frac{r_N}{R} = \left(\frac{t - t_P}{t_R} \right)^{1/2} \quad \text{where } t > t_P. \quad (50)$$

Finally we can also calculate the mean height of the gravity current at $t = t_R + t_P$ from the following equation:

$$\bar{h}_{t_R} = \frac{1}{R} \int_0^R h(y, t_R) dr = \xi_N^2 \left(\frac{Q_g}{S} \right)^{1/2} \int_0^1 \mathcal{H} dy = \xi_N^2 \left(\frac{Q_g}{S} \right)^{1/2} \bar{\mathcal{H}}. \quad (51)$$

From the numerical solution presented in figure 5, we find that $\bar{\mathcal{H}} \equiv \int_0^1 \mathcal{H} dy = 0.2641$. This result will be used in the following section where we describe the evolution of the flow for $t > t_R$.

4 First front

Once the gravity current reaches the impermeable sidewall, dense fluid begins moving upward and thus turns into a primarily vertical flow. As noted above, the interface between this ascending dense fluid and the ambient fluid is termed as the first front [2]. In the analogue Cartesian problem [17], we observe that the curvature of the first front is comparatively high initially but then relaxes as the first front approaches the plume source. We expect similar behaviour here and so focus on the variable of greatest dynamical significance, namely the mean elevation, \bar{h} , of the first front, averaged over the cross sectional area of the control volume. Further following Sahu & Flynn [17], we can apply a volume flux balance approach to find \bar{h} vs. time i.e.

$$\phi A \bar{U}_f(\bar{h}) = Q(H - \bar{h}). \quad (52)$$

Here $A = \pi R^2$ is the control volume cross-sectional area and $\bar{U}_f = \frac{d\bar{h}}{dt}$ is the mean advection speed of the first front, averaged over A . On substituting Q from (35) it can be shown that

$$\bar{h}_2 = H + x_0 - \left[(H + x_0 - \bar{h}_1)^{1/2} - \frac{(t_2 - t_1)}{A} \left(\frac{F_0 k \pi \alpha}{\nu \phi} \right)^{1/2} \right]^2 \quad (53)$$

where $\bar{h}_2 - \bar{h}_1$ is the mean vertical distance travelled by the first front over a time interval $t_2 - t_1$. By setting $\bar{h}_2 = H$ and $\bar{h}_1 = \bar{h}_{t_R}$, we can estimate the time, t_H , required by the first front to advect from the bottom to the top of the control volume. Thus

$$t_H = A \left(\frac{\nu \phi}{F_0 k \pi \alpha} \right)^{1/2} \left[(H + x_0 - \bar{h}_{t_R})^{1/2} - x_0^{1/2} \right]. \quad (54)$$

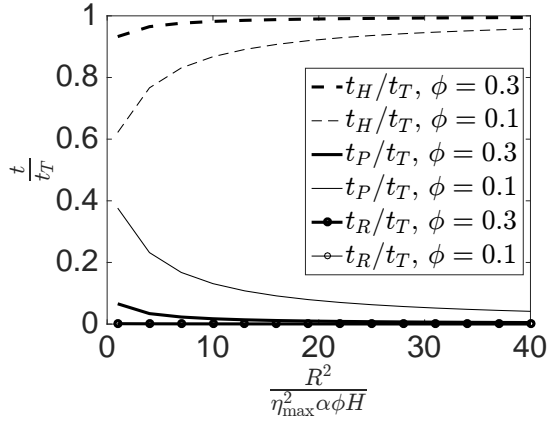


Fig. 6: Time scales $\frac{t_P}{t_T}$, $\frac{t_R}{t_T}$ and $\frac{t_H}{t_T}$ vs. $\frac{R^2}{\eta_{\max}^2 \alpha \phi H}$ for $\phi = 0.1, 0.3$.

5 Discussion

In the above sections we have separately considered solutions for the plume, gravity current and first front. The latter two solutions are applicable for a closed box or reservoir with an open upper boundary whose radius is significantly larger than the maximum plume radius i.e. $R \gg b_{\max}$. On substituting $b_{\max} = \eta_{\max}(\alpha \phi H)^{1/2}$, where $\eta_{\max} = 2.4048$, we get

$$\frac{R^2}{\eta_{\max}^2 \alpha \phi H} \gg 1. \quad (55)$$

For real geophysical flows, the horizontal length-scale is usually much larger than the vertical length scale; moreover $\phi < 0.38$ [14], $\alpha < 0.01$ m [4], and therefore the above criteria is well satisfied.

In the context of filling box flows, an important parameter is the time, t_T , required to completely fill the control volume void space with contaminated fluid. For $t > t_T$, we expect contaminated fluid overflow and, possibly, the advection of contaminated fluid above the elevation of the source. We calculate t_T by superposition, i.e.

$$t_T = t_P + t_R + t_H, \quad (56)$$

and focus attention on cases where (55) is valid. Plotting t_P , t_R and t_H vs. $\frac{R^2}{\eta_{\max}^2 \alpha \phi H}$ shows that t_H is typically much larger than either t_P or t_R (see figure 6). In our subsequent analysis, it is therefore appropriate to assume $t_T \approx t_H$ where t_H is given by (54) with $\bar{h}_{t_R} \rightarrow 0$. On the basis of this

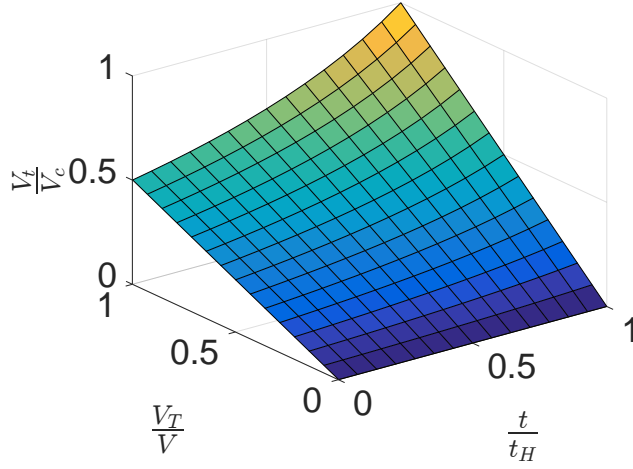


Fig. 7: [Colour online] Volume ratio V_t/V_c vs. t/t_H for various V_T/V (see equation 59).

approximation, it is possible to simplify (53). To wit

$$\bar{h} = \left[1 - \left(1 - \frac{t}{t_H} \right)^2 \right] H, \quad (57)$$

where \bar{h} is the mean height of the first front at time t . Thus, based on the time of injection, the mean depth and volume, V_c , of the contaminated layer can be straightforwardly predicted. In particular, V_c is given by

$$V_c = \phi A \bar{h} = \phi A \left[1 - \left(1 - \frac{t}{t_H} \right)^2 \right] H. \quad (58)$$

Conversely, the volume of injected source fluid is simply $V_t = Q_0 t$. With V_c and V_t to hand, we can compute their ratio from

$$\frac{V_t}{V_c} = \frac{V_T}{V} \frac{t}{t_H} \frac{1}{\left[1 - \left(1 - \frac{t}{t_H} \right)^2 \right]}, \quad (59)$$

where $V = V_c(t = t_H) = \phi A H$ is the pore volume and $V_T = V_t(t = t_H) = Q_0 t_H$ is the total volume of source fluid that can be injected up to the point of overflow.

Having calculated the volume of the contaminated layer, an estimate for the associated mean reduced gravity, \bar{g}'_c , can be obtained from simple mass balance, i.e.

$$\bar{\rho}_c V_c = \rho_0 V_t + \rho_\infty (V_c - V_t). \quad (60)$$

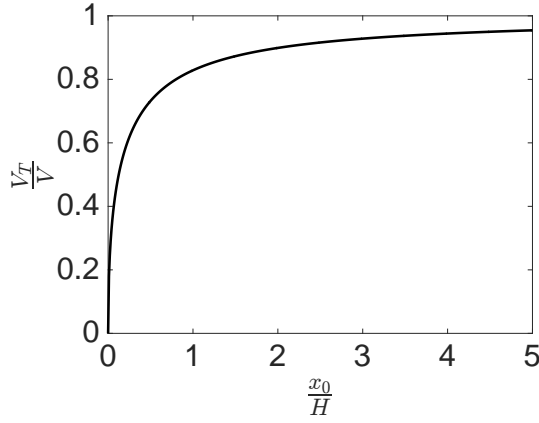


Fig. 8: Variation of the volume ratio V_t/V_c vs. x_0/H based on (62).

Here ρ_0 is the density of the source fluid, ρ_∞ is the reservoir fluid density at $t = 0$ and $\bar{\rho}_c$ is the mean density of the contaminated fluid. Manipulation of (60) gives

$$\frac{\bar{\rho}_c - \rho_\infty}{\rho_\infty} = \frac{\rho_0 - \rho_\infty}{\rho_\infty} \frac{V_t}{V_c} \quad \text{or} \quad \frac{\bar{g}'_c}{g'_0} = \frac{V_t}{V_c}, \quad (61)$$

where g'_0 is the reduced gravity of the source fluid.

Figure 7 shows the variation of V_t/V_c with t/t_H for various V_T/V . The maximum value of \bar{g}'_c , realized when $t = t_H$, is $g'_0 \frac{V_T}{V}$. Using the definitions of V_T , V , (34) and (54), it can be shown that V_T/V varies with x_0/H as

$$\frac{V_T}{V} = \frac{2x_0}{H} \left[\left(1 + \frac{H}{x_0} \right)^{1/2} - 1 \right] \quad (62)$$

(see figure 8). Thus as x_0/H increases, so too does (i) the total volume of fluid injected up to the point of overflow relative to the pore volume, and, (ii) the final mean reduced gravity of the contaminated layer relative to the source reduced gravity. In turn, and for constant k , ϕ and H , (34) shows that larger V_T/V is associated, respectively, with larger and smaller Q_0 and g'_0 whereby entrainment into the plume is comparatively modest. Whereas the latter conclusion applies for arbitrarily small g'_0 , it cannot necessarily be said that the former applies for arbitrarily large Q_0 : large source volumes fluxes are associated with large flow velocities so that the Reynolds number restriction $\text{Re} \lesssim \mathcal{O}(10)$ must eventually be violated. More specifically, let us suppose a source diameter of $d_0 = 2b_0$ so that the source discharge velocity is given by $U_0 = \frac{4Q_0}{\pi d_0^2}$. Now on recalling that the Reynolds number in porous media is

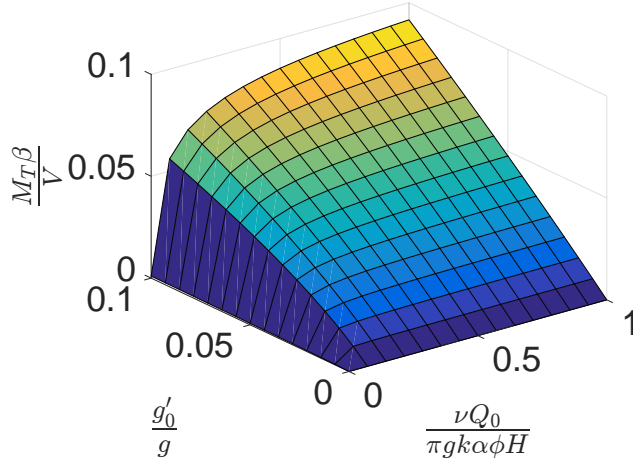


Fig. 9: [Colour online] Dimensionless mass of sequestered solute, $M_T\beta/V$, vs. $\nu Q_0/(\pi g k \alpha \phi H)$ for various g'_0/g (see equation 65).

defined as $\text{Re} = \frac{dU_0}{\nu}$, we can conclude

$$Q_0 \leq \frac{5\pi\nu d_0^2}{2d}. \quad (63)$$

Using above results, we can also calculate the mass, M_T , of solute that can be sequestered up until $t = t_H$ from

$$M_T = C_0 V_T \quad (64)$$

where $C_0 = \frac{g'_0}{g\beta}$ is the solute concentration of the source fluid – see (7). Then by combining (64) with (54) and (34), it can be shown that

$$\frac{M_T\beta}{V} = \frac{\nu Q_0}{2\pi g k \alpha \phi H} \left[\left(1 + \frac{4\pi g k \alpha \phi H}{\nu Q_0} \frac{g'_0}{g} \right)^{1/2} - 1 \right]. \quad (65)$$

The variation of $\frac{M_T\beta}{V}$ with $\frac{\nu Q_0}{\pi g k \alpha \phi H}$ and $\frac{g'_0}{g}$ is shown in figure 9, which suggests that for a fixed pore volume, V , a larger mass of solute can be sequestered for larger Q_0 and g'_0 .

6 Conclusions

In this manuscript a solution for filling box flows in axisymmetric porous media, which has closed lower horizontal and side vertical boundaries, is presented. This filling box model consists of three interrelated flow components:

(i) a negatively-buoyant axisymmetric plume, (ii) a radially spreading gravity current consisting of plume fluid discharged along the bottom boundary, and (iii) an upwelling-type flow that develops after the gravity current reaches the sidewalls.

The plume is assumed to be in Darcy regime with $Pe > \mathcal{O}(1)$; moreover, the flow is Boussinesq and miscible. In section 2, we derive a novel similarity solution assuming an unstratified ambient and present formulas for the plume volume flux, Q , reduced gravity, \bar{g}' , and the time, t_P , required for the plume to reach the bottom of the control volume respectively in (35), (36) and (40). It is found that Q and \bar{g}' vary respectively as $x^{1/2}$ and $x^{-1/2}$, whereas in previous studies with $Pe < \mathcal{O}(1)$ it has been shown that $Q \propto x$ and $\bar{g}' \propto x^{-1}$. We also argue that the new solution is more reasonable on physical grounds compared to the previous solution that Q and g' now depend on the buoyancy flux, viscosity and permeability, in addition to the porosity.

The above results are extended to derive a solution for the gravity current flow, where Q and \bar{g}' calculated at the bottom, $x = H$, of the control volume dictate the gravity current source volume flux and reduced gravity, respectively. We adapt the similarity solution of Lyle et al. [8], which is derived by combining Darcy's law and a mass balance equation. By synthesizing the similarity solutions for plume and gravity current flow, we present in figure 5 a solution for the gravity current height profile. Moreover (49) gives the corresponding amount of time, t_R , required for the gravity current front to reach the vertical sidewalls, which are located a radial distance R from the plume source.

Finally when $t > t_P + t_R$, the dense plume discharge starts advecting upward towards the source elevation. There exists an interface between this dense fluid and the overlying ambient fluid which is termed the first front. An equation that describes the temporal evolution of the first front is derived in section 4 based on a volume flux balance borrowed from Sahu & Flynn [17]. We thereby obtain an estimate for the time, $t_H \gg t_P, t_R$, required for the first front to advect all the way to the elevation of the source.

In section 5, we estimate via (59) the total volume, V_T , of source fluid that can be injected into a reservoir of pore volume $V = \phi AH = \phi \pi R^2 H$ up to the point of overflow. For fixed reservoir properties and dimensions, larger V_T can be realized by respectively increasing and decreasing the source volume flux and source reduced gravity (or concentration). The corresponding maximum reduced gravity of the contaminated layer, consisting of source fluid plus ambient fluid entrained into the descending plume, is given by (61). Finally (65) gives an expression for the total mass of solute sequestered, again up till the point of overflow. In contrast to V_T , figure 9 confirms that it is advantageous to increase both the source volume flux and source concentration assuming the objective is to sequester as much of the solute as possible.

The current research is conducted assuming a Darcy flow regime with uniform porosity and permeability and miscible fluids. However, real geological reservoirs are characterized by spatial variations in ϕ and therefore k . In future,

therefore, we will study filling box flows in porous medium with nonuniform permeability.

Acknowledgements The current research is supported by NSERC (Discovery Grant and RTI programmes) and Carbon Management Canada.

References

1. Underground injection wells for produced water disposal, USEPA Technical Workshops for the Hydraulic Fracturing Study: Water Resource Management. United States Environmental Protection Agency, Office of Research and Development (2011)
2. Baines, W.D., Turner, J.S.: Turbulent buoyant convection from a source in a confined region. *J. Fluid Mech.* **37**, 51–80 (1969)
3. Bolster, D.: The fluid mechanics of dissolution trapping in geologic storage of CO₂. *J. Fluid Mech.* **740**, 1–4 (2014)
4. Delgado, J.M.P.Q.: Longitudinal and transverse dispersion in porous media. *ICHEME* **85 (A9)**, 1245–1252 (2007)
5. Dudfield, P., Woods, A.W.: On the periodic injection of fluid into, and its extraction from, a porous medium for seasonal heat storage. *J. Fluid Mech.* **707**, 467–481 (2012)
6. Hunt, G.R., Kaye, N.G.: Virtual origin correction for lazy turbulent plumes. *J. Fluid Mech.* **435**, 377–396 (2001)
7. Lesage, S., Jackson, R.E.: Groundwater contamination and analysis at hazardous waste sites. Marcel Dekker, Inc. (1992)
8. Lyle, S., Huppert, H.E., Hallworth, M., Bickle, M., Chadwick, A.: Axisymmetric gravity currents in a porous medium. *J. Fluid Mech.* **543**, 293–302 (2005)
9. Nabi, S., Flynn, M.R.: The hydraulics of exchange flow between adjacent confined building zones. *Building and Environment* **59**, 76–90 (2013)
10. Neufeld, J.A., Vella, D., Huppert, H.E., Lister, J.R.: Leakage from gravity currents in a porous medium. part 1. a localized sink. *J. Fluid Mech.* **666**, 391–413 (2011)
11. Ogata, A.: Theory of dispersion in a granular medium. Tech. Rep. 411-1, U.S. Geol. Surv. Prof. Pap. (1970)
12. Oostrom, M., Rockhold, M.L., Thorne, P.D., Truex, M.J., Last, G.V., Rohay, V.J.: Carbon tetrachloride flow and transport in the subsurface of the 216-z-9 trench at the hanford site. *Soil Science Society of America* **6-4**, 971–984 (2007)
13. Parlange, M.B., Hopmans, J.W.: *Vadose Zone Hydrology*. Oxford University Press (1999)
14. Peters, E.J.: *Advanced Petrophysics*. Live Oak Book Company (2012)
15. Phillips, O.M.: *Flow and Reactions in Permeable Rocks*. 1st edn. Cambridge University Press (1991)
16. Roes, M.A., Bolster, D.T., Flynn, M.R.: Buoyant convection from a discrete source in a leaky porous medium. *J. Fluid Mech.* **755**, 204–229 (2014)
17. Sahu, C.K., Flynn, M.R.: Filling box flows in porous media. *J. Fluid Mech.* **782**, 455–478 (2015)
18. Scheidegger, A.E.: General theory of dispersion in porous media. *J. Geophys. Research* **66-10**, 3273–3278 (1961)
19. Shaffer, D.L., Chavez, L.H.A., Ben-Sasson, M., Castrillon, S.R., Yip, N.Y., Elimelech, M.: Desalination and reuse of high-salinity shale gas produced water: drivers, technologies, and future directions. *Environ. Sci. Technol.* **47**, 9569–9583 (2013)
20. Speer, K., Rona, K.: A model of an atlantic and pacific hydrothermal plume. *J. Geophys. Res. Oceans* **94**, 6213–6220 (1989)
21. Turcotte, D.L., Schubert, G.: *Geodynamics*. 3rd edn. Cambridge University Press (2014)
22. Wooding, R.A.: Convection in a saturated porous medium at large Rayleigh number or Péclet number. *J. Fluid Mech.* **15**, 527–544 (1963)
23. Woods, A.W.: Turbulent plumes in nature. *Annu. Rev. Fluid Mech.* **42**, 391–412 (2010)
24. Zakharov, Z.: Bessel functions and their applications to solutions of partial differential equations. Math 456 Lecture Notes, University of Arizona (2009)